

Figure S1, related to Figure 1: Microfluidic device designs, operation, calibration and stimulus sequence evaluation.

(A) Microfluidic device designs with 8, 16, or 24 channels for odorant stimulus delivery.

(B) Change in fluorescence intensity during delivery of 5 second step pulses of increasing concentrations of fluorescein dye, each followed by 5 seconds of water. Inset shows zoom-in of dashed box, indicating stimulus transition time of ~20 ms.

(C) Combination of on/off valve states required to generate the stimulus sequence highlighted in the shaded region of panel B. Rows indicate the stimulus type that a larva would experience. 1 and 0 indicate whether the valve is open or closed, respectively. C_W represents a water channel, C_{C1} and C_{C2} represent control channels 1 and 2 that allow stimulus switching, C_7 and C_8 represent odorant delivery channels which open prior to and during stimulus delivery.

(D) Images of fluorescein dye, representing an odorant stimulus, in the microfluidic device during each state shown in panel C (water, stimulus 7, stimulus 8). White cross indicates closed channels, star marks the location of a larva's ORN dendrites. Scale bar = 300 μm .

(E) Or35a-ORN responses to 0.5, 1, 2, 5, and 10 second pulse stimuli to a 10^{-5} dilution of the 3-octanol odorant. The maximum ORN response saturates when the odorant pulse is longer than 5 seconds.

(F) Or35a-ORN responses to increasing (top panel), primarily decreasing (middle panel), and random (bottom panel) concentration sequences of 3-octanol pulses, delivered at 5 seconds each. The response amplitude to each concentration level is independent of stimulus history.

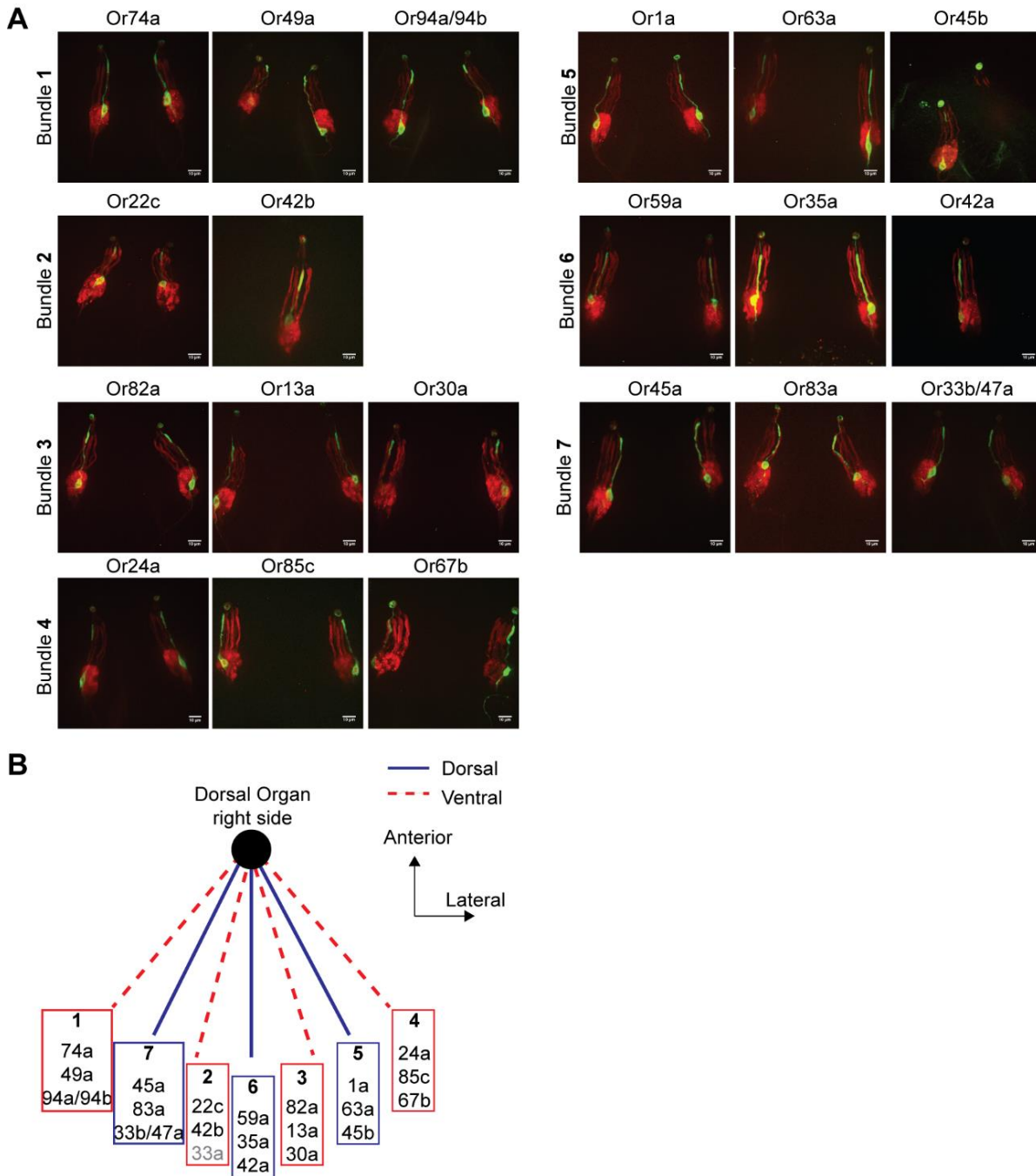


Figure S2, related to Figure 1: Anatomical map of ORN dendritic organization.

(A) Dendritic bundle location of each ORN in the larva. Larvae expressing *OrX>GFP*; *Orco>RFP*, where *OrX* is a specific olfactory receptor, were used to identify each ORN's dendritic bundle in green, while all ORNs were visible in red. We infer the vacancy in bundle 2 as the *Or33a*-ORN. No expression of *Or2a* and *Or7a* were observed in first instar larvae.

(B) Summary schematic of stereotyped ORN position in each dendritic bundle for right dorsal organ.

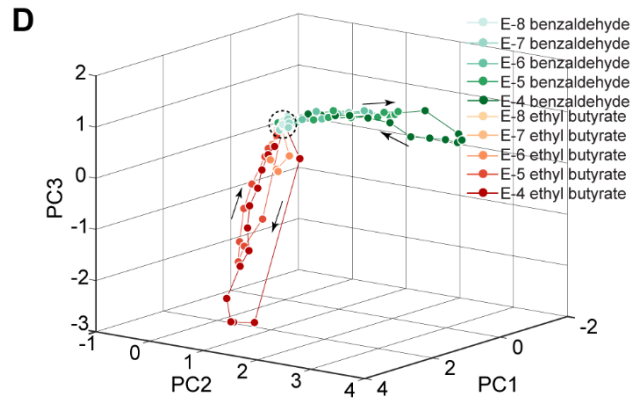
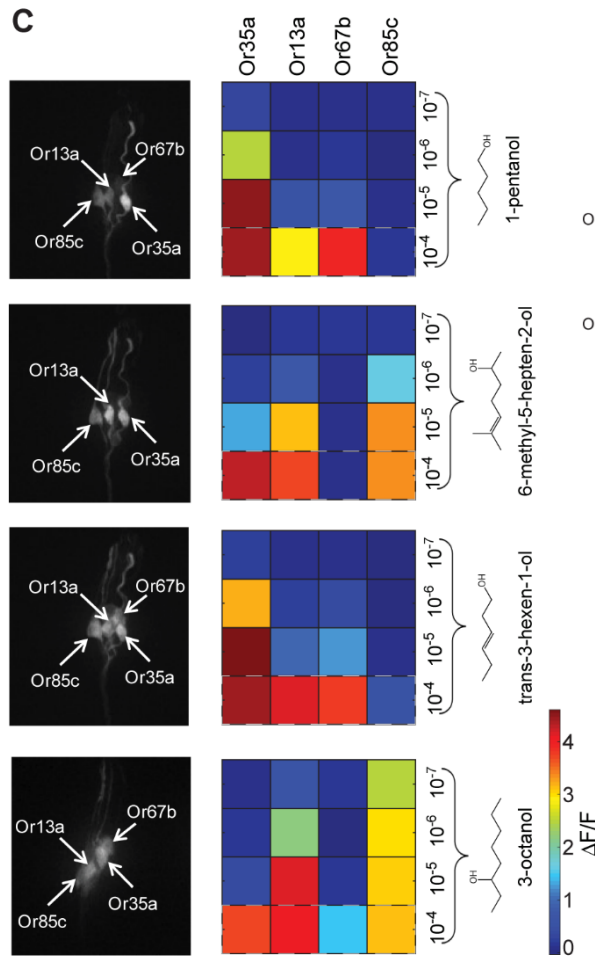
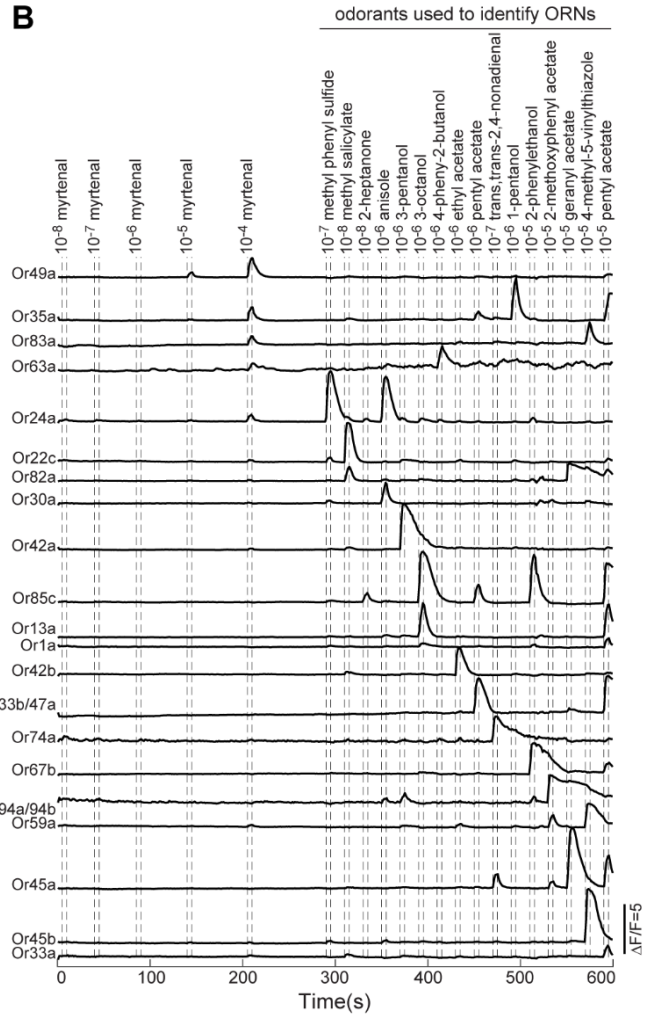
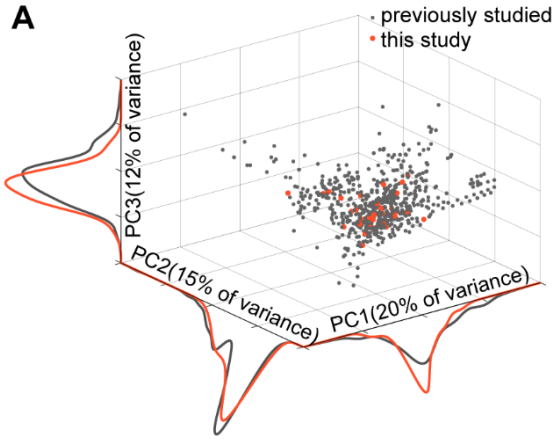


Figure S3, related to Figure 2: Odorant panel selection and ORN peak and dynamic responses.

(A) PCA of all odorants listed in the DoOR database (a collection of olfactory studies previously described in the *Drosophila* literature), where each odorant was described by the 32 most relevant molecular descriptors identified in Haddad et al., 2008. Gray dots correspond to the 690 monomolecular odorants catalogued in the DoOR database. Red dots correspond to the 35 odorants selected for this study. Distributions and breadth of selected odorants (red dots) closely match those previously used in the *Drosophila* literature (grey dots).

(B) Raw calcium activity traces for each of 21 ORNs in response to stimulus pulses of five concentrations of the odorant myrtenal followed by a panel of odorants that were used to identify each ORN.

(C) Heatmap of peak responses of four ORNs to four alcohol odorants, across four concentrations of each odorant. Neural images label the four ORNs in the dorsal organ ganglion during calcium imaging at the highest odorant concentrations.

(D) PCA of ORN population response over a 10~25 second period (during the 5 seconds of stimulus delivery and 5~20 seconds after stimulus offset) of two odorants, benzaldehyde and ethyl butyrate. Points are connected in temporal order (indicated by the arrows), forming distinct trajectories for each odorant. Dashed circle marks baseline starting position at onset of stimulus delivery.

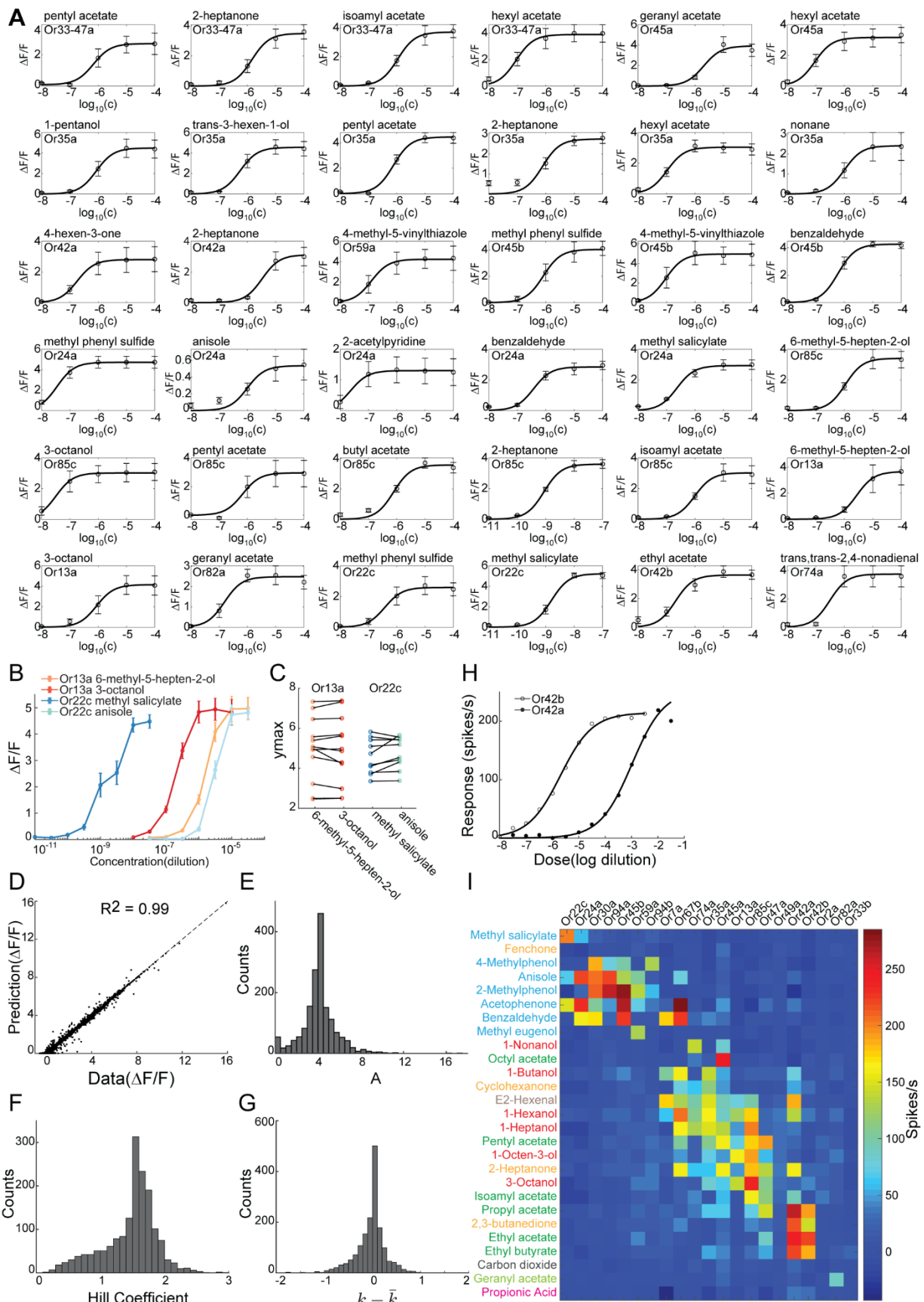


Figure S4, related to Figure 3: Hill curve fits to ORN dose-response data.

(A) Dose-response data for each of the 36 odorant-ORN pairs that reached saturation within the tested concentration range. All responses are fit to a Hill function with a common Hill coefficient.

(B) Dose-response curves for Or13a and Or22c ORNs, each in response to two different odorants ($n \geq 10$).

(C) Comparison of the maximum response amplitude (y_{max}) for each ORN to two different odorants. Each point indicates a separate animal. Colors of each point correspond to legend in panel B.

(D) Scatter plot of actual versus predicted response for each individual animal with a non-zero response value in Figure 2A. Dashed line indicates $y = x$. R^2 of the linear fit is 0.99.

(E-G) Distribution histograms of fitted amplitude, y_{max} (E), fitted Hill coefficient (F), and fitted variation in log sensitivity ($k = \log_{10}(1/EC_{50})$) (G), across all individuals.

(H) Plot of Or42a and Or42b ORN dose-response electrophysiology data from Kreher et al., 2008. Data from each ORN are fit to a Hill function with a Hill coefficient of 0.72 and 0.71 for Or42a and Or42b, respectively.

(I) Raw data of ORN firing rates from Kreher et al., 2008 reordered according to the simulated annealing method used to arrange **Figure 2A** (see **Methods**). Color of odorant name indicates type of functional group it contains (pink, organic acid; light green, terpene; gray, aldehyde; light orange, ketone; light blue, aromatic; red, alcohol; dark green, ester).

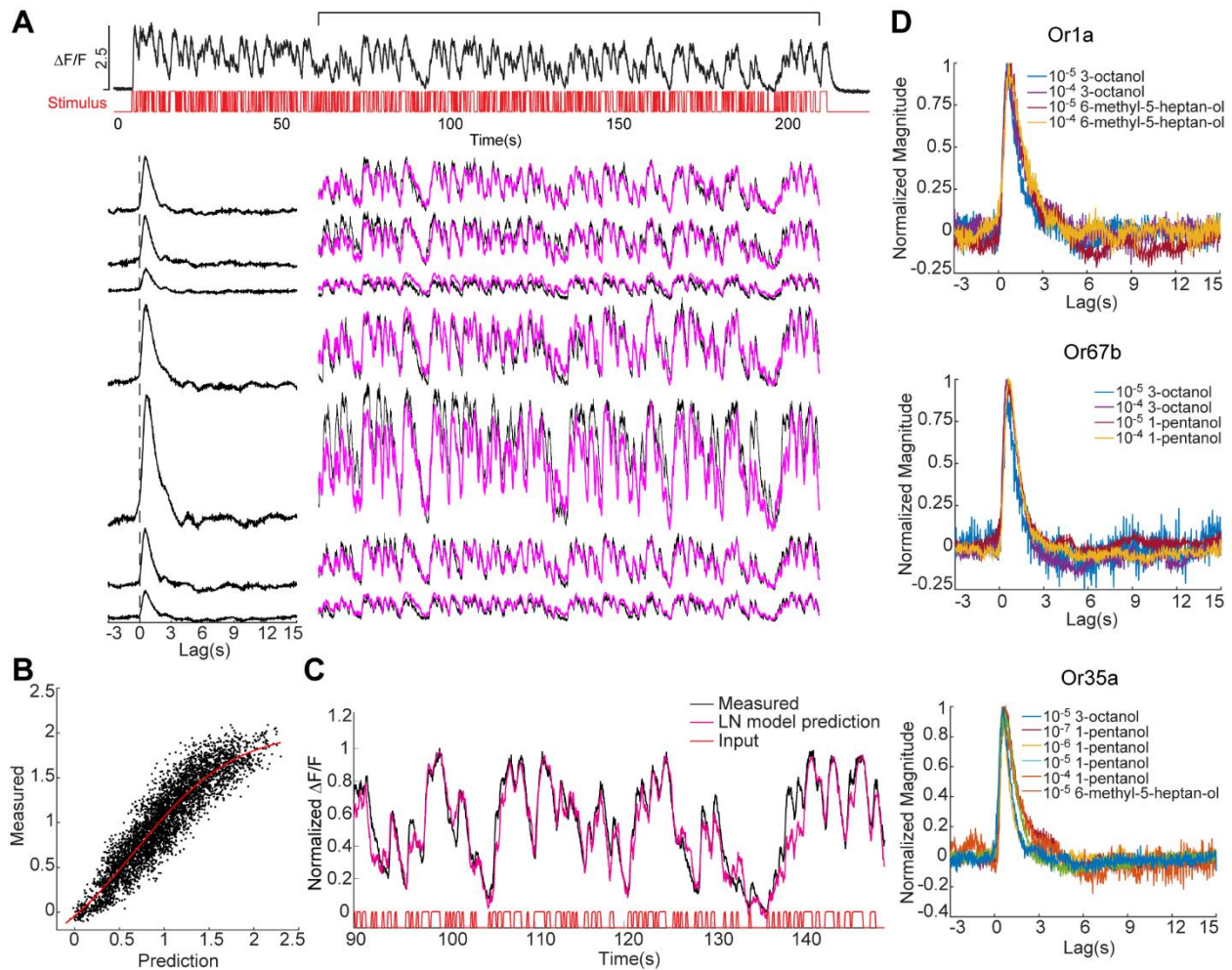


Figure S5, related to Figure 5: Characterization of ORN temporal response properties.

(A) Or42a-ORN responses (black curve) to a m-sequence of 10^{-7} dilution of 3-pentanol (shown in red). Each of seven traces (shown in black) is from a different animal. The response and temporal filter amplitudes vary from animal to animal (temporal filters shown to the left of each animal's response). Magenta traces show predicted response when the first animal's temporal filter and nonlinear function were rescaled to account for amplitude differences and then applied across all animals.

(B) Non-linear transfer function calculated by comparing measured and predicted responses using the linear filter of the first trial in panel A. Red curve follows the function of $y = \frac{a}{1+e^{-b(x-c)}} + d$, where $a = 2.7, b = 1.8, c = 0.68, d = 0.66$.

(C) Validation of the linear-nonlinear (LN) model by comparing predicted and measured responses to a novel m-sequence stimulus (generated using a different random seed from panel A). Example of a measured response (black) to the novel m-sequence stimulus (red). Magenta trace shows the LN model predicted response using parameters calculated from the same animal's response to the m-sequence stimulus shown in panel A.

(D) Normalized filters of three ORNs (Or1a, Or67b, and Or35a) responding to various odorant stimuli.

Odorant	Functional Group(s)	Component of Fruit or Plant	Behavioral studies in larvae	Physiology studies
acetal	acetal	fruit	Attractive (Mathew et al., 2013)	Mathew et al., 2013
nonane	alkane	plant oils, tomato		DoOR 2.0
ethyl acetate	ester	fruit	Attractive (Kreher et al, 2008)	DoOR 2.0
3-pentanol	alcohol	fruit		
geranyl acetate	ester, prenyl	leaf and plant oil	Aversive (Kreher et al, 2008)	Mathew et al., 2013, DoOR 2.0
4-hexen-3-one	enone (alkene + ketone)	fruit	Attractive (Mathew et al., 2013)	Mathew et al., 2013
ethyl butyrate	ester	fruit	Attractive (Kreher et al, 2008)	Asahina et al., 2009, DoOR 2.0
trans,trans-2,4-nonadienal	enal (alkene + aldehyde)	fruit	Attractive (Mathew et al., 2013)	Mathew et al., 2013
isoamyl acetate	ester	fruit	Attractive (Kreher et al, 2008)	Schubert et al., 2014
2-nonanone	ketone	leaf and seed oil	Attractive (Mathew et al., 2013)	Mathew et al., 2013
butyl acetate	ester	fruit	Attractive (personal communication Katrin Vogt)	Hoare et al., 2011, DoOR 2.0
hexyl acetate	ester	fruit		Chen et al, 2014, DoOR 2.0
2-heptanone	ketone	fruit	Attractive (Kreher et al, 2008)	Oppliger et al.2000, DoOR 2.0
3-octanol	alcohol	fruit and plants	Attractive (Kreher et al, 2008)	Mathew et al., 2013, DoOR 2.0
6-methyl-5-hepten-2-ol	alcohol, alkene	fruit	Attractive (Mathew et al., 2013)	Mathew et al., 2013
pentyl acetate	ester	fruit	Attractive (Kreher et al, 2008)	Mathew et al., 2013, DoOR 2.0
trans-3-hexen-1-ol	alcohol, alkene	leaf oil	Attractive (Mathew et al., 2013)	Mathew et al., 2013
1-pentanol	alcohol	fruit	Attractive (Mathew et al., 2013)	Mathew et al., 2013, DoOR 2.0
linalool	alcohol, prenyl	fruit and leaf oil		DoOR 2.0
4-methylcyclohexanol	alcohol			Oppliger et al.2000, DoOR 2.0
methyl salicylate	ester, phenol	leaf odor	Aversive (Kreher et al, 2008)	DoOR 2.0

benzyl acetate	ester, phenyl	fruit	Attractive (personal communication Katrin Vogt)	DoOR 2.0
4-phenyl-2-butanol	alcohol	fruit		DoOR 2.0
benzaldehyde	aldehyde	plant oils	Aversive (Kreher et al, 2008)	Chen et al, 2014, DoOR 2.0
methyl phenyl sulfide	thioether, phenyl	coffee	Attractive (Mathew et al., 2013)	Mathew et al., 2013
2,5-dimethylpyrazine	pyrazine	coffee	Attractive (Mathew et al., 2013)	Mathew et al., 2013, DoOR 2.0
2-acetylpyridine	pyridine, ketone	coffee, tea leaf	Attractive (Mathew et al., 2013)	Mathew et al., 2013, DoOR 2.0
anisole	ester, phenyl	not in fruit, in plant seed	Attractive (Kreher et al, 2008)	Mathew et al., 2013
4-methyl-5-vinylthiazole	thiazole, alkene	coffee and fruit	Attractive (Mathew et al., 2013)	Mathew et al., 2013
4,5-dimethylthiazole	thiazole	coffee and fruit	Attractive (Mathew et al., 2013)	Mathew et al., 2013, DoOR 2.0
(1R)-(-)-myrtenal	enal	plant oil and citrus fruits		DoOR 2.0
2-methoxyphenyl acetate	ester, ether, phenyl	not in fruit or plants	Attractive (Mathew et al., 2013)	Mathew et al., 2013
2-phenyl ethanol	alcohol, phenyl	fruit		
menthol	alcohol	plant oil	Aversive (personal communication with Katrin Vogt)	DoOR 2.0
pentanoic (valeric) acid	carboxylic acid	fruit		DoOR 2.0

Table S1, related to Figure 2: Description of odorants.

List of 35 odorants used in this study, followed by their molecular functional groups, presence in the natural environment, and examples of their use in the previous literature to study behavior and physiology in the *Drosophila* larva.

	power law	log-normal	exponential	stretched exponential	power law with cutoff
$f(x)$	$x^{-\alpha}$	$\frac{1}{x} \exp\left[-\frac{(\ln x - \mu)^2}{2\sigma^2}\right]$	$e^{-\lambda x}$	$x^{\beta-1} e^{-\lambda x^\beta}$	$x^{-\alpha} e^{-\lambda x}$
$p(x) = C f(x)$	$(\alpha - 1)x_{\min}^{\alpha-1}$	$\sqrt{\frac{2}{\pi\sigma^2}} \left[\operatorname{erfc}\left(\frac{\ln x_{\min} - \mu}{\sqrt{2}\sigma}\right)\right]^{-1}$	$\lambda e^{\lambda x_{\min}}$	$\beta \lambda e^{\lambda x_{\min}^\beta}$	$\frac{\lambda^{1-\alpha}}{\Gamma(1-\alpha, \lambda x_{\min})}$
parameters w.r.t $x_{\min} = 4.2 \times 10^4$	$\alpha = 1.42$	$\mu = 4.8$ $\sigma = 4.9$	$\lambda = 2.9 \times 10^{-8}$	$\beta = 0.08$ $\lambda = 2.4 \times 10^{-4}$	$\alpha = 1.38$ $\lambda = 3.4 \times 10^{-10}$
	$p = \mathbf{0.17}$	LR = -1.1 $p = 0.2$	LR = 272 $p = 1$	LR = -1.1 $p = 0.2$	LR = -0.8 $p = 0.2$

Table S2, related to Figure 3: Comparison of sensitivity fit using different distributions.

Comparison of fitting ORN population sensitivities using power law versus other common heavy-tailed distributions. Statistically significant p-values are denoted in bold. Other heavy-tailed distributions are not significantly better than the power law.